The effect of a serotonin-induced dissociation between spiking and perisynaptic activity on BOLD functional MRI

Alexander Rauch*†, Gregor Rainer*, and Nikos K. Logothetis*†‡

*Max Planck Institute for Biological Cybernetics, Spemannstrasse 38, D-72076 Tübingen, Germany; and ‡Division of Imaging Science and Biomedical Engineering, University of Manchester, Manchester M13 9PT, United Kingdom

Edited by Marcus E. Raichle, Washington University School of Medicine, St. Louis, MO, and approved March 10, 2008 (received for review January 11, 2008)

The relationship of the blood oxygen-level-dependent (BOLD) signal to its underlying neuronal activity is still poorly understood. Combined physiology and functional MRI experiments suggested that local field potential (LFP) is a better predictor of the BOLD signal than multiunit activity (MUA). To further explore this relationship, we simultaneously recorded BOLD and electrophysiological activity while inducing a dissociation of MUA from LFP activity with injections of the neuromodulator BP554 into the primary visual cortex of anesthetized monkeys. BP554 is a 5-HT1A agonist acting primarily on the membrane of efferent neurons by potassium-induced hyperpolarization. Its infusion in visual cortex reliably reduced MUA without affecting either LFP or BOLD activity. This finding suggests that the efferents of a neuronal network pose relatively little metabolic burden compared with the overall presynaptic and postsynaptic processing of incoming afferents. We discuss implications of this finding for the interpretation of BOLD activity.

5-HT1A | BP554 | local field potentials | multiunit activity

The blood oxygen-level-dependent (BOLD) signal represents a complex response controlled by different parameters, including blood oxygenation, cerebral blood flow, and cerebral blood volume, all in turn reflecting regional increases in metabolism due to enhanced neural activity. Although the existence and importance of this neurometabolic and neurovascular coupling have long been acknowledged, the actual relationship between neuronal activity and the ensuing hemodynamic response signal is still far from being completely understood. An important pertinent question is the contribution of different processing stages to hemodynamic responses. In principle, brain structures are conceptualized as information-processing entities, with an input, a local processing capacity, and an output. Yet, although such a scheme can often successfully describe the function of subcortical nuclei, its implementation in different areas of cortex is anything but straightforward. This is mainly so because the local cortical connectivity reveals strong excitatory and inhibitory recurrence, and the output reflects changes in excitation–inhibition balance rather than simple feed-forward integration of inputs (1).

Autoradiography studies have long suggested that the "perisynaptic" activity, mostly representing the input and local processing in cortex, accounts for the lion's share of metabolic energy demands (2). For instance, the greatest 2-deoxyglucose uptake occurs in the neuropil, i.e., in areas rich in synapses, dendrites, and axons, rather than in cell bodies. When cell bodies and axon terminals of neurons are in different structures, as is the case with the cells in the supraoptic and paraventricular nuclei of the hypothalamus, only the structures involving presynaptic terminals (in this case the posterior pituitary gland) exhibit increased glucose consumption during electrical microstimulation (3). Similarly, the highest density of cytochrome oxidase (an enzyme of the respiratory chain) is found in somatodendritic regions that are adjacent to axon terminals (4, 5).

Simultaneous measurements of intracortical activity and functional MRI in the non-human primate have confirmed these findings by demonstrating that the local field potential (LFP) generated by a local neuronal network are more closely related to the BOLD signal than the multiunit activity (MUA) of the same network, although both electrical measures of neuronal activity are correlated with the BOLD signal (6). The LFP is a mass signal that reflects a whole population of excitatory or inhibitory postsynaptic potentials as well as a number of integrative processes, including somatic and dendritic potentials with their ensuing afterpotentials and voltage-dependent membrane oscillations (2–4, 7).

The decisive observation underlying the conclusions of these fMRI experiments (6) was the characteristic hemodynamic response in cases of cortical LFP–MUA dissociation. In that study, hemodynamic responses were not reduced at many recording sites in the absence of neuronal spiking, but there remained strong stimulus-induced modulation of the field potentials. A similar but experimentally induced dissociation had been reported previously in the cerebellum of rats in a study combining electrophysiology with laser Doppler flowmetry (8), i.e., with regional measurements of cerebral blood flow. These investigators stimulated the parallel fibers of cerebellum while recording Purkinje cell activity. Measurements of LFPs, single-unit activity, and changes in cerebral flow showed that both LFPs and CBF may increase at the same time that spiking activity ceases (8, 9). Most recently a similar LFP–MUA dissociation was also reported in the cortex of cats in studies directly measuring neural activity and tissue oxygenation at a high spatiotemporal resolution (10). These authors demonstrated a strong coupling between LFPs and changes in tissue oxygen concentration in the absence of spikes. All of these observations suggest that the perisynaptic, i.e., dendrosomatic elements of neuronal networks are the sites of enhanced metabolic activity, a large part of which might serve to restore the perturbed ionic gradients in the postsynaptic membranes (7, 9).

Here we set out to test the differential contributions of LFP and MUA to the fMRI signal, doing so directly in concurrent electrophysiological and fMRI experiments by selectively decreasing the MUA in primary visual cortex with injections of a 5-HT1A agonist. BP554 is a centrally active 5-HT1A agonist whose primary function is to raise the spike threshold of

NEUROSCIENCE

Author contributions: A.R. and N.K.L. designed research; A.R. performed research; A.R. and G.R. analyzed data; and A.R., G.R., and N.K.L. wrote the paper.

The authors declare no conflict of interest.

This article is a PNAS Direct Submission.

Freely available online through the PNAS open access option.

†To whom correspondence may be addressed. E-mail: arauch@tuebingen.mpg.de or nikos.logothetis@tuebingen.mpg.de.

This article contains supporting information online at www.pnas.org/cgi/content/full/0800312105/DCSupplemental.

pyramidal neurons by hyperpolarization (11). The hyperpolarization triggered by the 5-HT1A receptor is mostly driven by a potassium current, stabilizing the membrane of pyramidal neurons at a hyperpolarized level and reaching a spiking threshold only under a much heavier synaptic load (12, 13). In the macaque cortex, the 5-HT1A receptors show a discrete localization on the initial segment of the axon hillock in layer-3 and layer-5 pyramidal neurons (14). This localization is ideally suited for the 5-HT1A receptors to perform a sort of gatekeeper function for the output of neuronal networks, thereby controlling spiking activity. BP554 is therefore expected to primarily affect the output side of the neuronal network by reducing MUA. The LFP, on the other hand, should remain largely intact because thalamic and corticocortical inputs continue to stream to the network and keep generating local synaptic activity. Our experiment allows us to assess pharmacologically whether the BOLD signal is more faithfully represented by MUA or LFP activity.

BP554 injections were performed in the primary visual cortex (V1) of anesthetized monkeys during a visual stimulation protocol, allowing us to assess the changes in visually induced activity. To identify possible drug-induced changes to the BOLD signal with high sensitivity, we used independent component analysis (ICA) on the imaging data. We have previously shown that spatial ICA provides a sensitive method to quantify the impact of local injections on the BOLD signal (15). In particular, this method can robustly identify injection-related changes in visual stimulus-induced BOLD modulation and at the same time delineate their spatial extent. A preliminary report on the action of the 5HT agonist using a different experimental protocol was published elsewhere (16).

Results

We induced activity in the primary visual cortex (V1) by using a block paradigm consisting of a rotating polar checkerboard stimulus lasting 32 s followed by an isoluminant gray blank period of equal length [see supporting information (SI) Fig. S1]. After a baseline period lasting four blocks of visual stimulation, we performed local injection of the 5HT1A agonist BP554 using a single dose of 10 μl at a concentration of 100 μM. We analyzed the fMRI data using spatial ICA (see *Materials and Methods*). We focus here on independent components (ICs) showing robust correlation with the visual stimulation during the baseline period. In Fig. 1*A* we show, for a single experiment, the three ICs and their spatial distribution in V1 in three slices around the injector. The injector is marked by a blue arrow and was placed in cortical layer IV/V. Voxels corresponding to each of the ICs were located in cortical regions within the field of view (FOV) and surrounding the injector. Fig. 1*B* shows the time course of IC_1; the arrow indicates the time of injection at the end of the fourth block of visual stimulation. No effect on the time course of IC_1 can be detected after the injection of BP554. The modulation in response to the visual stimulus is plotted in Fig. 1 *C–E* for the three ICs. The ordinate of the graphs denotes the visual modulation in percent of baseline values (100%), such that a reduction in modulation due to the injection would result in a decrease of modulation after the time of injection. None of the modulation plots shows significant reduction after the injection. Statistical analyses confirm that modulation was in fact similar during the baseline period (0–4.3 min) and a period after the injection (6.5–14.2 min) (*t* test: IC_1, $P = 0.70$; IC_2, $P = 0.64$; IC_3, $P = 0.29$). The injection of BP554 thus has no significant effect on any of the groups of voxels surrounding the injector that were identified by ICA.

A group analysis summarized in Fig. 2 confirmed that this observation was made reliably across all experiments. In Fig. 2 *A–C* the average visual modulation for the three ICs is shown in percentages, and the time of injection is again indicated by an arrow. When the baseline period (0–4.3 min) was compared with

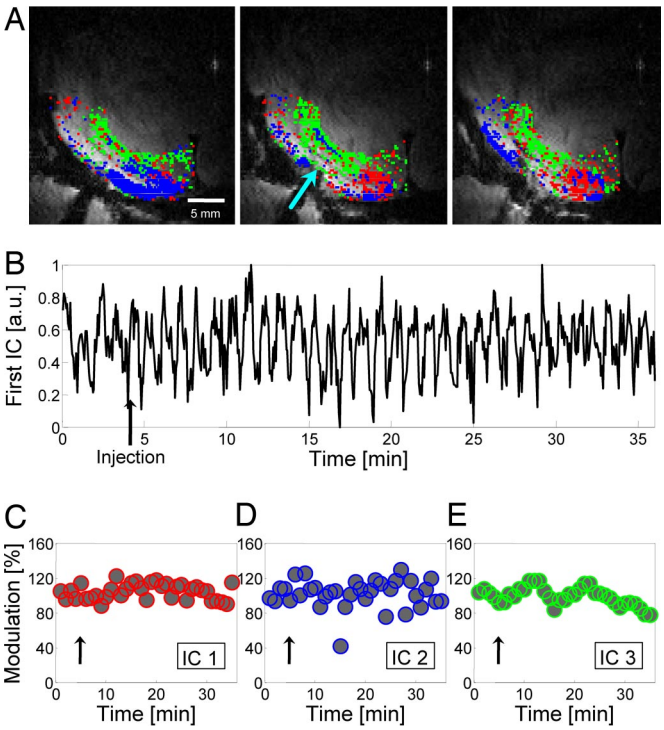

Fig. 1. Single-trial results for BOLD activity. (*A*) Three panels showing slices of 1-mm thickness and interslice separation of 1 mm including regions of primary visual cortex around the injector in *Center*. Each panel shows voxel distributions corresponding to the three ICs, IC_1 (red), IC_2 (blue), and IC_3 (green). (*B*) Time course of IC_1. The black arrow marks the time of the injection of 10 μl of BP554. (*C*) Visual modulation for IC_1. (*D*) Visual modulation for IC_2. (*E*) Visual modulation for IC_3. In *C–E* the time of the injection is indicated by a black arrow.

the postinjection period (6.5–14.2 min), there was no significant change in visual modulation for any of the ICs (*t* test: IC_1, $P = 0.76$; IC_2, $P = 0.51$; IC_3, $P = 0.52$). This analysis shows that the three selected ICs remain unaffected by the injection and continue to display robust stimulus-induced modulation. To confirm that these effects observed at the level of ICs were also true for the raw fMRI data, we repeated this analysis on the BOLD data corresponding to each of the ICs. Fig. 3 shows the raw data corresponding to each of the ICs. The baseline period (0–4.3 min) compared with the postinjection period (6.5–14.2 min) did not show any significant change in visual modulation (IC_1, raw BOLD *t* test, $P = 0.31$; IC_2, raw BOLD *t* test, $P = 0.29$; IC_3, raw data *t* test, $P = 0.11$). This indicates that effects for the raw BOLD data were in close agreement to the effects seen in the ICs, and both signals were not significantly affected by BP554 injections. Thus, even the highly sensitive spatial ICA method did not reveal any voxel groups that might have been strongly affected by the injection. However, it might still be the case that the amount of remaining visual stimulus-induced BOLD modulation in each of the ICs still correlates with the distance from the injector. This would indicate that the drug injection does have a quantifiable effect on the BOLD signal. In Fig. S2 and *SI Text* we show that this was in fact not the case.

Given that BOLD signals were unaffected by the injection, we proceeded to analyze neuronal activity at the level of LFP and MUA to examine which of these signals was a better predictor of BOLD activity. Fig. 4 shows the electrophysiological recordings of the experiment corresponding to the fMRI results presented in Fig. 1. The electrophysiological signals were bandpassed into two frequency ranges: MUA from 800 Hz to 3,000 Hz and LFP from 24 Hz to 90 Hz. Fig. 4*A* shows the time course

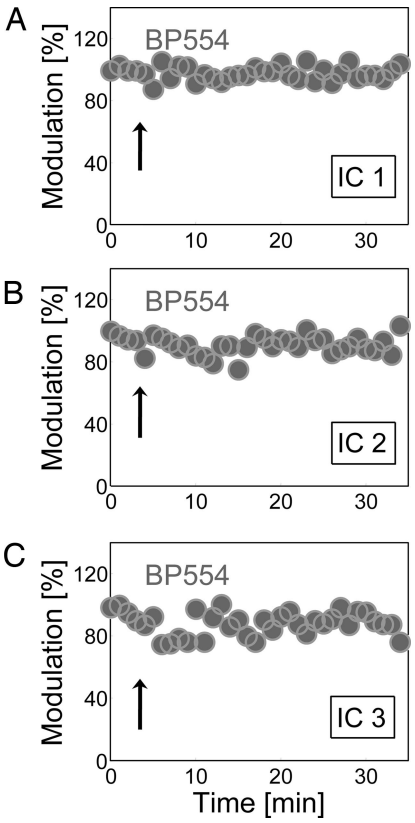

Fig. 2. Group analysis of BOLD activity. Average visual modulation for IC_1 (*A*), for IC_2 (*B*), and for IC_3 (*C*), respectively. The time of the injection of 10 μl of BP554 is indicated by a black arrow.

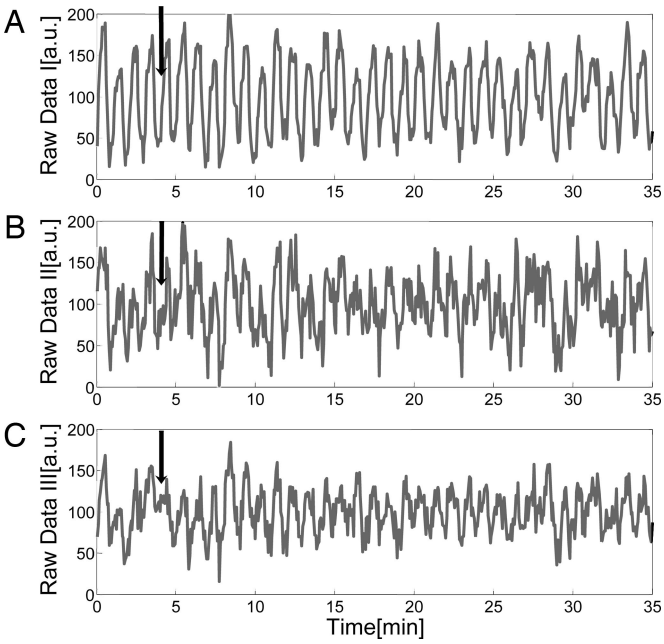

Fig. 3. Averaged raw data of the BOLD activity selected by ICA. (*A*) Averaged raw data of the BOLD signal corresponding to IC_1. (*B*) Averaged raw data corresponding to IC_2. (*C*) Averaged raw data corresponding to IC_3.

of the MUA: a clear decrease in visual modulation is evident shortly after the injection of BP554. The effect is transient and shows a robust recovery after the injection. The MUA returned to its initial modulation levels ≈15 min after the injection. Fig. 4*B* shows the corresponding LFP activity, and it is evident that only a short-lasting decrease in activity occurs ≈8 min after the injection. Apart from this, LFP activity is by and large unaffected by the drug injection. Fig. 4 *C* and *D* shows the visual modulation of the MUA and the LFP activity, and the substantial effect of BP554 on MUA is evident in a reduction of visual modulation by 86% (t test, $P < 0.01$) after the injection (6.5–14.2 min) compared with the baseline period. By contrast, for the same comparison there is no effect on visual modulation of LFP activity (t test, $P = 0.99$).

Fig. 5 shows the mean MUA and LFP time courses and their visual modulation for all experiments with combined electrophysiology and fMRI. Fig. 5*A* shows the mean MUA time course, with a clear decrease in visual modulation after the injection of BP554. In contrast, the modulation of LFP activity shown in Fig. 5*B* remains unaltered. Note that both MUA and LFP show a change in baseline activity after the time of the injection. This change in baseline common to both signals is likely to have an origin other than the modulation-related changes that are the focus of the present study. The drug-induced changes in modulation can be better demonstrated by plotting the modulation over time rather than the actual time course of the signal. Fig. 5*C* shows exactly this for both MUA and LFP. The visual modulation of the MUA after the injection decreases by 34% with a recovery time of ≈10 min, much like the MUA modulation changes observed in Fig. 4. A comparison of the modulation during the baseline period (0–4.3 min) with that of the postinjection period (6.5–14.2 min) showed that the decrease in the visual modulation of MUA was significant (t test, $P < 0.05$) whereas that of the LFP activity was not (t test, $P = 0.56$). In these analyses we focused on two specific aspects of the neuronal activity, namely the frequency ranges associated with MUA and LFP activity. For completeness, we show the impact of the injection on the entire frequency spectrum in Fig. S3 and discuss these effects in *SI Text*.

These findings suggest that LFP and BOLD signals remain closely coupled during BP554 injections, whereas both of these signals are temporarily uncoupled from MUA. To directly visualize this across all experimental sessions, we produced scatter plots comparing the impact of BP554 injections on the MUA–LFP, MUA–BOLD, and LFP–BOLD relationships. Fig. 6 shows an experiment-by-experiment analysis of the observed three signals, MUA, LFP, and BOLD, whereby BOLD modulation is estimated as the average across the three ICs. We compared visual modulation during the postinjection period (6.5 min to 14.2 min) with values during the recovery epoch (30.1 min to 34.5 min) In Fig. 6*A*, MUA shows a clear reduction in visual modulation during the postinjection period (squares) whereas LFP does not (triangles). This difference is significant (t test, $P < 0.05$). After recovery from the drug effect MUA and LFP show similar distributions (t test, $P = 0.48$). In Fig. 6*B* MUA again shows a clear reduction of visual modulation compared with BOLD activity (t test, $P < 0.05$). After recovery from the drug effect there is no longer a significant difference between the distributions of BOLD and MUA (t test, $P = 0.83$). Finally, in Fig. 6*C* there is little reduction in the visual modulation of both BOLD and LFP activity after the injection of BP554, and no specific distribution can be found either after the injection or in the recovery phase for the two signals (t test, after injection $P = 0.44$ and after recovery $P = 0.36$). Taken together, this suggests that during the drug application MUA diverges or uncouples from both LFP and BOLD activity, whereas the coupling between LFP and BOLD remains intact.

As a control, we compared the results of BP554 injections with those of saline injections. We found that saline injections had no

NEUROSCIENCE

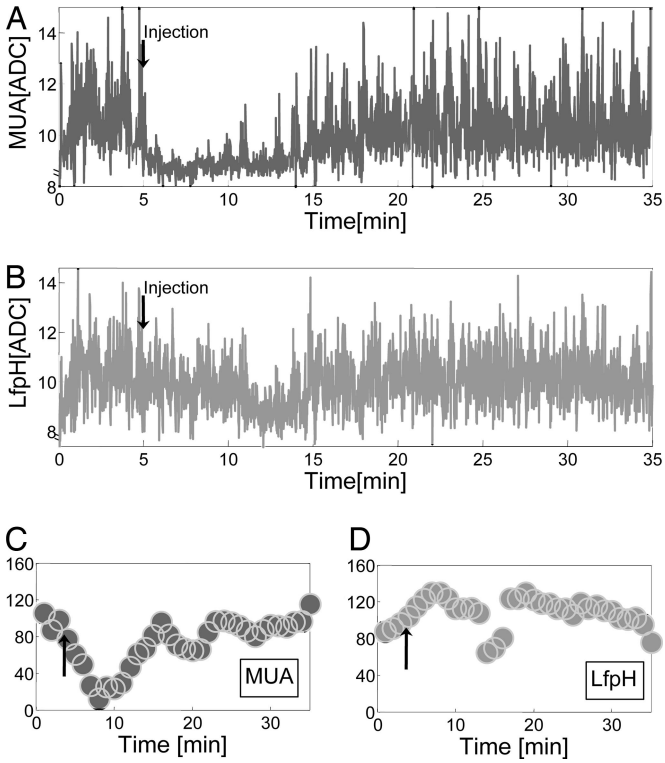

Fig. 4. MUA versus LFP single trial. (*A*) Time course of MUA associated with injection of 10 μl of BP554, with injection indicated by a black arrow. (*B*) Time course of LFP associated with injection of 10 μl of BP554, with injection indicated by a black arrow. (*C* and *D*) Visual modulation of MUA (*C*) and visual modulation of LFP (*D*). Injections are indicated by black arrows.

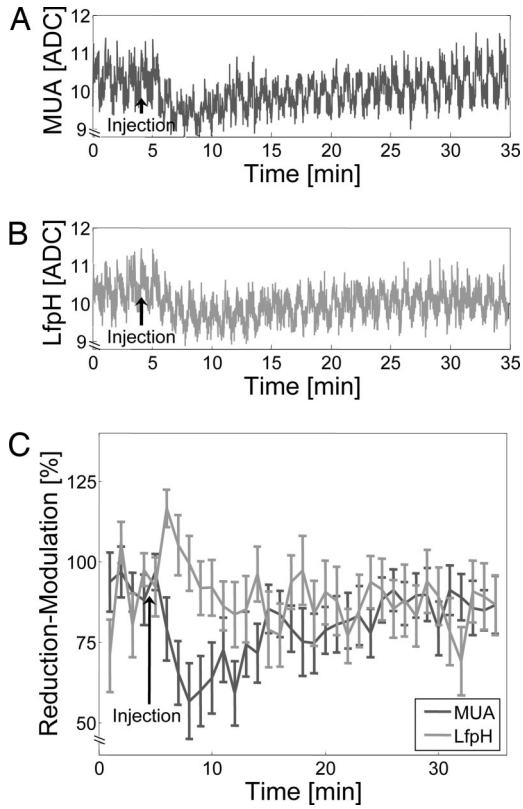

Fig. 5. MUA versus LFP group analysis. (*A*) Average time course of MUA associated with injection of 10 μl of BP554, with injection indicated by a black arrow. (*B*) Average time course of LFP associated with injection of 10 μl of BP554, with injection indicated by a black arrow. (*C*) Average visual modulation of MUA and average visual modulation of LFP.

systematic effect on the BOLD signal or on the electrophysiological signals (see Fig. S4 and *SI Text*).

Discussion

We described the effects of the 5-HT1A agonist BP554 (100 μM solution) on neural and BOLD activity in the primary visual cortex of monkeys. The agonist was used to induce dissociation between LFP and MUA activity. This dissociation is due to the fact that BP554 selectively hyperpolarizes pyramidal neurons in cortex through an increase in potassium conductivity that clamps the neuronal membrane close to this ion's reversal potential (13, 17). Because of this pharmacological specificity and the narrow distribution of 5-HT1A receptors around the axon hillock of these neurons, the 5-HT1A agonist BP554 acts as a gatekeeper for the output of the neuronal network (MUA) (14, 18). We were able to show that the main effect of BP554 is exerted on MUA, whereas LFP remains largely unaffected. Simultaneous fMRI during the recording of neuronal signals and drug application allowed us to address the question: Which of the two measures of neuronal activation is a better predictor of BOLD signal levels? We found that, during the temporary uncoupling of MUA from LFP activity, the BOLD signal indeed is well predicted by LFP activity. The robust decreases in MUA levels during drug application by contrast do not have an appreciable impact on the BOLD signal in cortical areas around the injector. This functional relationship is consistent with previous observations (6, 8, 19). To the best of our knowledge, however, this is the first study reporting the effects of different types of neural activity on the BOLD fMRI signal under the condition of experimentally induced LFP–MUA dissociation.

Our findings demonstrate, once again, that increases in the fMRI signal may not necessarily be interpreted as showing an increase in the activity of the area's projection neurons—the neurons typically monitored during extracellular recording in experimental animals. Naturally, increases in the field potentials are often coupled with increases in spiking and in hemodynamic responses. This is most pronounced in experiments in which responses to a simple sensory stimulus are studied. In fact, it is remarkable that LFP–MUA dissociations occur during such simple experimental designs and even in the anesthetized animal. Neuroimaging in studies of human cognitive capacities, however, in which a cortical area might be strongly influenced by neuromodulation (e.g., as a result of attention, arousal, or short-term memory), could show that LFP and MUA may vary to different extents or even in opposite directions.

The occasional discussion about the relationship of spikes to BOLD suffers from a certain amount of contention seeking where none is warranted. For one, LFP and MUA cannot be always regarded as independent measures of activity, and their dissociation usually speaks to the relative contribution of these signals to the BOLD signal in the cortex. The strong recurrent excitatory and inhibitory loops of the typical cortical microcircuit predict correlations between these signals, each of which may then be also correlated with the local BOLD signal levels (6, 20, 21). Should, however, the excitatory and inhibitory conductances show proportional increases or decreases, hemodynamic responses may strongly change with little difference in the spiking of stimulus-selective projection neurons. Here we have examined BOLD levels in the primary visual cortex (V1) during visual stimulation. V1 receives visual signals from the lateral geniculate nucleus, and these synaptic inputs continue to arrive during the entire experimental session regardless of drug appli-

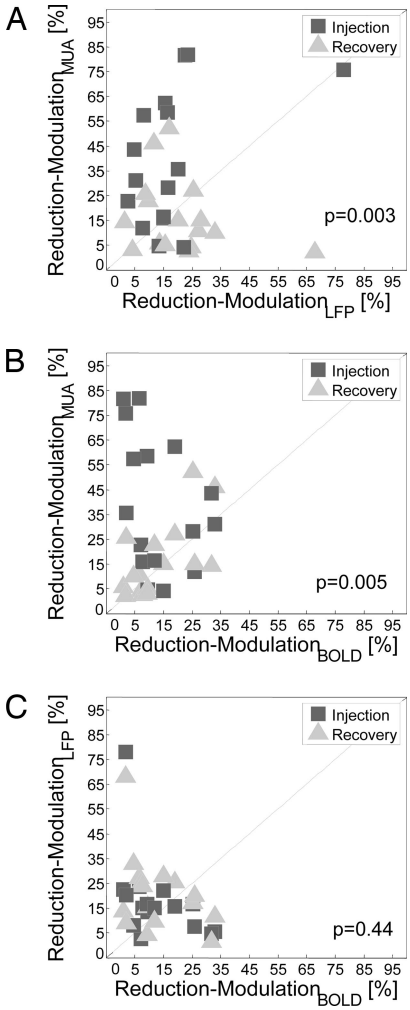

Fig. 6. Comparison of MUA, LFP, and BOLD activity. (*A*) Average visual modulation reduction after injection of 10 μl of BP554 for MUA versus LFP, with the postinjection period (6.5 min to 14.2 min) indicated by rectangles and the recovery period (35.1 min to 39.5min) indicated by triangles. (*B*) Average visual modulation reduction for MUA versus BOLD activity; symbols are as in *A*. (*C*) Average visual modulation reduction for LFP versus BOLD activity; symbols are as in *A*.

cation in V1, because the drug applied in V1 cannot directly affect the neurons in the distant thalamic nucleus. Our model system thus allows us to examine drug effects in V1 under conditions where synaptic inputs continue to arrive, and the reported results corroborate indeed the notion that synaptic activity is in general a better predictor of metabolic demand than local spiking.

In the present study we used ICA to analyze the BOLD imaging data because we had previously found it to be more sensitive for the delineation of drug effects than traditional methods. In a previous study examining the effects of lidocaine on neural and vascular signals (15), ICA was able to identify meaningful clusters of voxels on the basis of changes in the time course of the voxels at and around the injection site. The study also showed that the distribution of lidocaine-affected voxels was often anisotropic. ICA showed clear advantages over a traditional distance-to-injector-based correlation analysis because it accounted for the anisotropic distribution and estimated this information directly from experimental data sets with no prior assumptions on the possible distribution of the affected voxels. We used the same methodology here to study effects of BP554 to maximize our chances of observing injection-related effects on the BOLD signal. We suggest that, particularly for pharmacological MRI studies, ICA provides a valuable tool for delineating and describing effects in the BOLD signal.

Finally, our present observations have some interesting implications for medical research. In specific, variations of endogenous levels of serotonin can occur because of different cognitive states or as a result of brain disorders. Our findings suggest that such variations could have an appreciable impact on BOLD signals observed in functional imaging experiments involving human subjects by action of the 5-HT1A receptor. Indeed, there is now increasing evidence that 5-HT1A receptors are involved in the pathology of schizophrenia. In human prefrontal cortex the density of these receptors increases by up to 80% in this disorder (22, 23). Given our results, one might expect that the activation of the pathologically increased 5-HT1A receptors through their action primarily on MUA would lead to a decrease in the output of the prefrontal neural networks without disrupting local processing. In this view, local processing might be relatively unimpaired, but the output of prefrontal circuits would not be available to control activity in target brain regions. Because BOLD signals couple to LFP under serotonergic manipulation, these pathological changes in information processing would be difficult to detect by using fMRI. This is consistent with recent evidence (24, 25) indicating that the overall amplitude of BOLD responses is undisturbed in patients with schizophrenia. Note that these studies did observe changes in BOLD temporal dynamics, suggesting that subtle aspects of fMRI activation, other than signal intensity, may provide clues to the output of local networks. Further research is needed to uncover the neuronal and metabolic mechanisms underlying BOLD signal generation.

In summary, we have shown that the activation of an endogenous 5-HT1A receptor, which in a relay-like function depresses the efferent output of neuronal networks (MUA), does not affect visual modulation of the BOLD signal, nor does it lead to significant reductions in afferent neuronal processing (LFP). We can conclude that in this brain state the LFP serves as a more reliable indicator of the cortical BOLD signal than MUA.

Materials and Methods

Three male rhesus monkeys (*Macaca mulatta*) aged 4–6 years and weighing 5–7 kg were used. The surgical operations and anesthesia procedures have been described in detail elsewhere (26, 27). The experiments were approved by the local authorities (Regierungspräsidium) and were in full compliance with the guidelines of the European Community for the care and use of laboratory animals (EUVD 86/609/EEC).

Injections. We used three independent injection lines driven by three separate HPLC pumps (M6; VICI). The three independent lines allowed us to switch between different solutions in successive trials during one experiment. All lines were monitored by high-precision flow meters (Sensirion) controlling the exact applied volume and the actual flow. We used BP554 as a 5-HT1A agonist. We observed no side effects during our experiments, and BP544 is to our knowledge not used clinically. A stock solution of 100 mM BP554 in DMSO was prepared and further diluted with a solution on the basis of artificial cerebrospinal fluid (ACSF) to a final concentration of 100 μM BP554. The pH was adjusted with NaOH to 7.25. The ACSF was composed of 148.19 mM NaCl, 3.0 mM KCl, 1.40 mM $CaCl_2$, 0.80 mM $MgCl_2$, 0.80 mM Na_2HPO_4, and 0.20 mM NaH_2PO_4. The unmodified ACSF solution was also used as a control solution. These chemicals, including BP554 and DMSO, were purchased from Sigma-Aldrich. BP554 injections were delivered at depths corresponding to cortical layers IV/V.

Recording Electrodes. The recording electrodes and injectors were custom-made; the injector consisted of a triple-barrel glass tube to keep the lines separated until the very tip of the injector. Electrode and injector formed one unit to assure placement at same depth. The resistance of the recording electrodes was in the range of 0.6 MΩ.

Electrophysiology. The monkeys had an implanted recording chamber on the primary visual cortex, V1. These chambers are made of PEEK (a nonmagnetic polymer) and were custom-milled for an optimal fit on the skull. The amplifiers for the electrophysiological recordings were custom-made and already had an analog compensation mechanism for the gradient noise from the scanner. The precleaned signal was then read in by an analog–digital (AD) converter with 16-bit resolution (National Instruments). The AD converter was linked directly to a PC running a real-time QNX operating system, where the signal was stored. However, the denoising process was not yet complete at this point, so additional offline cleaning of the data sets was necessary to completely remove gradient artifacts. This was done with custom-written code based on principal component analysis in Matlab (MathWorks).

Magnetic Resonance Imaging. Images were acquired with a 4.7-tesla Bruker BioSpec 47/40v scanner with a 40-cm-diameter bore (Bruker). Customized, small radio frequency coils with an inner diameter of 30 mm were used as transceivers and were directly positioned around the recording chamber. They were optimized for increased sensitivity over the chosen region of interest of primary visual cortex (V1). For functional imaging we used Gradient Echo EPI with a FOV of 76.8 to 48.0 mm, a slice thickness of 1 mm, and in-plane resolution of 0.3×0.375 mm^2. We used a multishot EPI with eight segments, flip angle 30°, TR/TE 500/18 ms. A total of 592 volumes were acquired in each experiment. Slices were oriented parallel to the injector and perpendicular to the cortical surface with the center slice containing the injector. Anatomical reference scans were made by using a high-resolution GEFI sequence with in-plane resolution of 0.15×0.19 mm for a FOV of 76.8×48.0 mm. Special care was taken in the shimming process to achieve good homogeneity of the magnetic field by using FASTMAP (28) with a shim volume of 12 mm^3 positioned in the area of the electrode tip.

Visual Stimulation. Visual stimuli were presented binocularly by using a γ-corrected SVGA fiber optic system (AVOTEC; Silent Vision) with a resolution of 640×480 voxels and a frame rate of 60 Hz. Hard contact lenses were inserted to bring the plane of stimulus into focus (hard PMMA lenses; Wöhlk). The visual stimulation resulted in a good activation of primary visual cortex V1. Our stimulation protocol consisted of blocks of visual stimulation using a rotating polar checkerboard stimulus $10° \times 10°$ in size lasting 32 s followed by an isoluminant gray blank period of equal length. Checkerboard rotation direction was reversed every 8 s to minimize adaptation of the BOLD and neural signals. In the injection scan the drugs were applied after the fourth repetition of an on–off sequence; the injection lasted between 2 and 3 min, and the duration of the entire scan was 39.5 min corresponding to 37 blocks of visual stimulation.

Data Analysis. We applied spatial ICA to the imaging data, allowing the determination of spatially independent brain topographies, each of which is associated with a characteristic distribution measured over the repeated acquisition of volumes and whose weighted sum recovers the original imaging data (29, 30). Using the Matlab toolbox fastICA (31), we estimated a number of IC time courses and determined the voxels that strongly contributed to each IC by selecting those voxels whose component values exceeded a set threshold value. Voxel activation distributions were normalized such that the SD $\sigma = 1$, and we used a cutoff SD value of $\eta = 2$. For each experimental data set between 10 and 30 ICs were produced, three to five of which showed robust visual-stimulus-induced modulation during the baseline period before injection. For each experiment, we selected the three ICs that were most strongly activated by visual stimulation and named them IC_1, IC_2, and IC_3. The correlation coefficients of the selected components with the visual stimulation paradigm across all experiments (mean $\pm$ SD) were as follows: IC_1, 0.54 ± 0.18; IC_2, 0.36 ± 0.13; IC_3, 0.35 ± 0.11. We considered only the first three ICs because statistical analyses revealed that correlation coefficients of IC_4 (0.263 ± 0.091) and IC_5 (0.217 ± 0.081) were already significantly lower than 0.35 (mean of IC_3) over all experiments ($P < 0.01$ for IC_4, and $P < 0.001$ for IC_5) and were not consistently activated by the visual stimulus. Modulation was estimated by subtracting IC values during the baseline period (blocks 11–16) from corresponding values during stimulus (blocks 3–8) to take account of the hemodynamic lag. Our IC selection evidently made no assumptions regarding the signal changes that followed the agonist injection because it relied on the baseline time window before injection.

The electrophysiological signals were band-passed into two frequency ranges: MUA from 800 Hz to 3,000 Hz and LFP from 24 Hz to 90 Hz. The power of the two bands was calculated for time bins corresponding to the sampling of the BOLD signal, namely 592 time points (volumes) corresponding to an experimental duration of 39.5 min. Then the visual modulation was computed for each block of visual stimulation by subtracting the power values during the baseline period (blocks 9–16) from corresponding power values during the stimulus (blocks 1–8).

ACKNOWLEDGMENTS. This work was supported by the Max Planck Society, Grants 01GQ0711 and 01EV0701 from the German Ministry of Education and Research, Swiss National Science Foundation Grant PBBSB-106816, and the M. and W. Lichtenstein Foundation (Switzerland) (A.R.). G.R. is a Deutsche Forschungsgemeinschaft Heisenberg Investigator (RA-1025/1-2).

1. Douglas RJ, Martin KA (2004) Neuronal circuits of the neocortex. *Annu Rev Neurosci* 27:419–451.
2. Jueptner M, Weiller C (1995) Review: Does measurement of regional cerebral blood flow reflect synaptic activity? Implications for PET and fMRI. *NeuroImage* 2:148–156.
3. Schwartz WJ, *et al.* (1979) Metabolic mapping of functional activity in the hypothalamo-neurohypophysial system of the rat. *Science* 205:723–725.
4. Di Rocco RJ, Kageyama GH, Wong-Riley MT (1989) The relationship between CNS metabolism and cytoarchitecture: A review of 14C-deoxyglucose studies with correlation to cytochrome oxidase histochemistry. *Comput Med Imaging Graphics* 13:81–92.
5. Kageyama GH, Wong-Riley M (1986) Laminar and cellular localization of cytochrome oxidase in the cat striate cortex. *J Comp Neurol* 245:137–159.
6. Logothetis NK, Pauls J, Augath M, Trinath T, Oeltermann A (2001) Neurophysiological investigation of the basis of the fMRI signal. *Nature* 412:150–157.
7. Logothetis NK, Wandell BA (2004) Interpreting the BOLD signal. *Annu Rev Physiol* 66:735–769.
8. Mathiesen C, Caesar K, Akgoren N, Lauritzen M (1998) Modification of activity-dependent increases of cerebral blood flow by excitatory synaptic activity and spikes in rat cerebellar cortex. *J Physiol* 512:555–566.
9. Mathiesen C, Caesar K, Lauritzen M (2000) Temporal coupling between neuronal activity and blood flow in rat cerebellar cortex as indicated by field potential analysis *J Physiol* 523:235–246.
10. Viswanathan A, Freeman RD (2007) Neurometabolic coupling in cerebral cortex reflects synaptic more than spiking activity. *Nat Neurosci* 10:1308–1312.
11. Matsuda T, *et al.* (1989) Agonist activity of a novel compound, 1-[3-(3,4-methylenedioxyphenoxy)propyl]-4-phenyl piperazine (BP-554), at central 5-HT1A receptors. *Eur J Pharmacol* 170:75–82.
12. Ma L, Shalinsky MH, Alonso A, Dickson CT (2007) Effects of serotonin on the intrinsic membrane properties of layer II medial entorhinal cortex neurons. *Hippocampus* 17:114–129.
13. Beique JC, *et al.* (2004) Serotonergic regulation of membrane potential in developing rat prefrontal cortex: Coordinated expression of 5-hydroxytryptamine (5-HT)1A, 5-HT2A, and 5-HT7 receptors. *J Neurosci* 24:4807–4817.
14. Azmitia EC, Gannon PJ, Kheck NM, Whitaker-Azmitia PM (1996) Cellular localization of the 5-HT1A receptor in primate brain neurons and glial cells. *Neuropsychopharmacology* 14:35–46.
15. Rauch A, Rainer G, Augath M, Oeltermann A, Logothetis NK (2008) Pharmacological MRI combined with electrophysiology in non-human primates: Effects of Lidocaine on primary visual cortex. *NeuroImage* 40:590–600.
16. Logothetis NK (2003) MR imaging in the non-human primate: Studies of function and of dynamic connectivity. *Curr Opin Neurobiol* 13:630–642.
17. Tanaka E, North RA (1993) Actions of 5-hydroxytryptamine on neurons of the rat cingulate cortex. *J Neurophysiol* 69:1749–1757.
18. Czyrak A, Czepiel K, Mackowiak M, Chocyk A, Wedzony K (2003) Serotonin 5-HT1A receptors might control the output of cortical glutamatergic neurons in rat cingulate cortex. *Brain Res* 989:42–51.
19. Attwell D, Iadecola C (2002) The neural basis of functional brain imaging signals. *Trends Neurosci* 25:621–625.
20. Mukamel R, *et al.* (2005) Coupling between neuronal firing, field potentials, and FMRI in human auditory cortex. *Science* 309:951–954.
21. Raichle ME, Mintun MA (2006) Brain work and brain imaging. *Annu Rev Neurosci* 29:449–476.
22. Gurevich EV, Joyce JN (1997) Alterations in the cortical serotonergic system in schizophrenia: A postmortem study. *Biol Psychiatry* 42:529–545.
23. Bantick RA, Deakin JF, Grasby PM (2001) The 5-HT1A receptor in schizophrenia: A promising target for novel atypical neuroleptics? *J Psychopharmacol* 15:37–46.
24. Ford JM, Johnson MB, Whitfield SL, Faustman WO, Mathalon DH (2005) Delayed hemodynamic responses in schizophrenia. *NeuroImage* 26:922–931.
25. Fox MD, Snyder AZ, McAvoy MP, Barch DM, Raichle ME (2005) The BOLD onset transient: Identification of novel functional differences in schizophrenia. *NeuroImage* 25:771–782.
26. Logothetis NK, Guggenberger H, Peled S, Pauls J (1999) Functional imaging of the monkey brain. *Nat Neurosci* 2:555–562.
27. Logothetis N, Merkle H, Augath M, Trinath T, Ugurbil K (2002) Ultra high-resolution fMRI in monkeys with implanted RF coils. *Neuron* 35:227–242.
28. Gruetter R (1993) Automatic, localized in vivo adjustment of all first- and second-order shim coils. *Magn Reson Med* 29:804–811.
29. Stone JV (2002) Independent component analysis: An introduction. *Trends Cognit Sci* 6:59–64.
30. McKeown MJ, Sejnowski TJ (1998) Independent component analysis of fMRI data: Examining the assumptions. *Hum Brain Mapp* 6:368–372.
31. Hyvarinen A (1999) Fast and robust fixed-point algorithms for independent component analysis. *IEEE Trans Neural Netw* 10:626–634.